ACS APPLIED MATERIALS & INTERFACES

Research Article

Cite This: ACS Appl. Mater. Interfaces 2019, 11, 2768−2781

www.acsami.org

Biodegradable Polymer-Coated Multifunctional Graphene Quantum Dots for Light-Triggered Synergetic Therapy of Pancreatic Cancer

Chengbin Yang,[†] Kok Ken Chan,[‡] Gaixia Xu,[*,†] Mingjie Yin,[‡] Guimiao Lin,[§] Xiaomei Wang,[§] Wei-Jen Lin,[∥] Muhammad Danang Birowosuto,[⊥] Shuwen Zeng,[⊥] Takashi Ogi,[#] Kikuo Okuyama,[#] Fitri Aulia Permatasari,[#,¶] Ferry Iskandar,[¶] Chih-Kuang Chen,[*,▽] and Ken-Tye Yong[*,‡]

[†]Guangdong Key Laboratory for Biomedical Measurements and Ultrasound Imaging, School of Biomedical Engineering, Health Sciences Center, and [§]Department of Physiology, School of Basic Medical Sciences, Health Sciences Center, Shenzhen University, Shenzhen 518060, China

[‡]School of Electrical and Electronic Engineering, Nanyang Technological University, Singapore 639798, Singapore

[∥]Department of Fiber and Composite Materials, Feng Chia University, Taichung 40724, Republic of China

[⊥]CINTRA CNRS/NTU/THALES UMI 3288, Research Techno Plaza, 50 Nanyang Drive, Singapore 637553, Singapore

[#]Department of Chemical Engineering, Graduate School of Engineering, Hiroshima University, Higashi Hiroshima 7398527, Japan

[¶]Department of Physics, Faculty of Mathematics and Natural Sciences, Institut Teknologi Bandung, Bandung 40132, Indonesia

[▽]Department of Chemical and Materials Engineering, National Yunlin University of Science and Technology, Yunlin 64002, Republic of China

Supporting Information

ABSTRACT: In this work, we reported the synthesis of an engineered novel nanocarrier composed of biodegradable charged polyester vectors (BCPVs) and graphene quantum dots (GQDs) for pancreatic cancer (MiaPaCa-2 cells) therapy applications. Such a nanocarrier was utilized to co-load doxorubicin (DOX) and small interfering ribonucleic acid (siRNA), resulting in the formation of GQD/DOX/BCPV/siRNA nanocomplexes. The resulting nanocomplexes have demonstrated high stability in physiologically mimicking media, excellent K-ras downregulation activity, and effective bioactivity inhibition for MiaPaCa-2 cells. More importantly, laser light was used to generate heat for the nanocomplexes via the photothermal effect to damage the cells, which was further employed to trigger the release of payloads from the nanocomplexes. Such triggered release function greatly enhanced the anticancer activity of the nanocomplexes. Preliminary colony formation study also suggested that GQD/DOX/BCPV/siRNA nanocomplexes are qualified carrier candidates in subsequent in vivo tests.

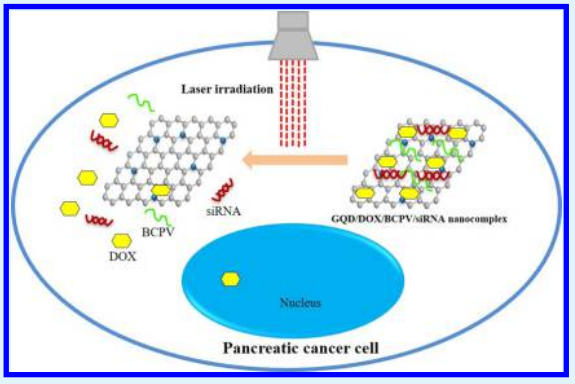

KEYWORDS: *graphene quantum dots, BCPV, light-triggered, siRNA, DOX, pancreatic cancer*

1. INTRODUCTION

Pancreatic cancer progressed from the fourth to the third deadliest cancers in 2017, with a yearly increase of 53 070 new pancreatic cancer cases diagnosed and 41 780 deaths associated with pancreatic cancer.[1] Doxorubicin (DOX) has been the first-line drug for pancreatic cancer treatment. However, it is difficult to achieve the desired therapeutic effect through sole DOX treatment due to drug resistance.[2,3] To improve the cancer therapeutic effect, the current research trend has shifted from mono-chemotherapy to synergistic therapy.[4−6] We have noticed that the high mortality rate of pancreatic cancer is closely associated with K-ras gene mutation, which is found in approximately 90% of pancreatic cancer patients.[7] Activated K-ras regulates a number of downstream signal molecules including Raf kinase, Ral guanine nucleotide exchange factors, and phosphoinositide 30-kinase to yield pleiotropic cellular effects that regulate cell growth, differentiation, and survival. The point mutation at codon 12 in the K-ras gene keeps the constitutive GTPase activity and locks the protein to the guanosine triphosphate (GTP)-bound "on" state. Then, the mutant K-ras gene will endow the cells with tumor phenotype and eventually cause cancer formation.[8] The downregulation of mutant K-ras expression has been reported to promote cell apoptosis, inhibit cell metastasis, and reduce drug resistance.[8] Hence, mutant K-ras gene can be considered as a potential therapeutic target for suppressing the develop-

Received: September 17, 2018
Accepted: December 27, 2018
Published: December 27, 2018

DOI: 10.1021/acsami.8b16168
ACS Appl. Mater. Interfaces 2019, 11, 2768−2781

ment of pancreatic cancer.[9] Ribonucleic acid interference (RNAi) is an effective method to inhibit mutant K-ras gene expression by targeted cleavage of K-ras messenger RNA (mRNA) using small interfering RNA (siRNA) molecules in pancreatic cancer cells.[10] However, the application of RNAi faces a series of challenges. Naked siRNA is negatively charged, exhibiting large molecular weight, and easily degraded by ribonuclease. Without a carrier, siRNA is unable to penetrate into the hydrophobic cell membrane by itself. Thus, we first utilized cationic polymer-coated graphene quantum dots (GQDs) as a DOX and K-ras siRNA co-delivery carrier for combining the chemotherapy and gene therapy on pancreatic cancer treatment.

Semiconductor quantum dots (QDs) have been developed over the past decades by virtue of their high potential applications in bioimaging, drug delivery, and medical diagnostics.[11] QDs have been widely reported as excellent cell imaging agents because of their bright and stable fluorescence character.[12−15] However, their poor water solubility, photobleaching properties, and potentially high toxicity significantly hampered their applicability in the biomedical field.[11] Recently, carbon-based fluorescent nanomaterials, such as GQDs,[16] carbon dots,[17−19] and graphene oxide (GO),[20,21] have attracted significant attention because of their unique optical and biocompatible traits under physiological conditions. Such traits are greatly beneficial for biological applications. Among the different carbon-based materials, GQDs, fragments of single- or few-layer two-dimensional graphene with generally a very small lateral dimension, have attracted great interest in various biomedical applications, such as drug delivery,[22] biomedical imaging,[23,24] and photodynamic therapy.[25] Recent studies confirmed that GQDs exhibit no apparent toxicity in vitro and in vivo owing to its high biocompatible property, whereas GO appeared to have toxicity, which even caused death to mice due to the GO aggregation.[26] Meanwhile, GO has very low fluorescence efficiency, which limits its application on tracking GO in an individual cell.[27] On the other hand, the presence of active groups on GQDs allows them to be conjugated with different functional groups for developing a multifunctional drug delivery platform.[16] The mentioned features ensure GQDs to be an ideal carrier probe for simultaneous treatment and monitoring for cancer cells. Synthetic strategies of GQDs can be resulting from two routes: bottom-up (cleavage and exfoliation of bulk graphene-based materials, such as graphite) and top-down (multistep oxidative condensation reactions in organic solutions starting from polycyclic aromatic compounds, such as citric acid) methods.[16] The top-down methods are generally hindered by the obvious lack of morphological control and harsh, environmentally unfriendly, and high-cost procedures. In contrast, the bottom-up approaches can provide precise control on the morphology, size, and shape of the synthesized nanoparticles (NPs). Using the bottom-up approaches, GQDs are capable of possessing superior optical properties and have been extensively applied in in vitro and in vivo imaging and sensing.[16,28] Accordingly, a bottom-up approach was implemented in this study. The highly water-dispersible GQDs were prepared in large quantities using a hydrothermal method with citric acid as the carbon source.

On the basis of the outstanding performances of GQDs, for example, facile fabrication, excellent biocompatibility, large surface area, and easy conjugation with biomolecules,[29−33] GQDs thus were selected as the nanocarrier in this study. In order to realize the co-loading function of DOX and siRNA, the selection of a suitable modification polymer on GQDs is vital. Polyethylenimine (PEI) has been widely used to modify versatile NPs to form drug and gene co-loading carriers.[34] Nevertheless, PEI had some serious drawbacks, such as long-term toxicity and nondegradability under physiological conditions.[35] To address the problems, PEGylation of PEI became a frequently used approach. The covalent attachment of polyethylene glycol (PEG) can contribute to avoiding the immune system, reducing immunogenicity and antigenicity, and prolonging blood circulatory time.[36] However, PEGylation requires elaborate studies on selecting suitable structure of PEG, adjusting the proper chain number and applying a workable coupling chemistry technique, which greatly increase the difficulty in selecting the ideal PEG.[37] To tackle those challenges, we synthesized well-defined biodegradable cationic polylactides with pendant tertiary amine groups as the modified polymer for GQDs, named as biodegradable charged polyester vectors (BCPVs). In our previous study, BCPV exhibited a tunable charge density property, biocompatibility, and negligible cytotoxicity.[9,36,38] Specifically, we have demonstrated that BCPVs are capable of degrading into a small molecular weight species after 1 week in an aqueous environment. Having such a character,[9,39] BCPVs after administration can be further eliminated out of human body, thus enabling the repeated administration of therapeutic genes when BCPVs as their vectors. BCPV is highly effective in encapsulating siRNAs to form a particle-like structure and providing the protection of siRNA from enzymatic digestion. Meanwhile, BCPV facilitates the cell uptake of the loaded siRNA and assists the siRNA escape from endosome into cytosol, which is an essential mechanism for RNAi-based therapeutic application.[9,40] Hence, having a positively charged property and great biodegradability, BCPV was supposed to be an ideal candidate for modifying GQDs. Accordingly, the BCPV-functionalized GQDs were employed to co-load DOX and siRNA to study the synergistic anticancer activity of gene/chemo combinational therapy.

Light, as an external stimulus, offers a facile approach to control drug release at a desired time and space. The controlled drug release is crucial to boost drug efficacy in cancer treatment while minimizing derivative side effects.[41,42] Photothermal therapy (PTT) therefore has attracted huge interest in recent years as a result of its minimally invasive nature for maximally destroying cancerous cells but minimally damaging the surrounding healthy tissues.[43,44] Nanoparticulated systems having photothermal properties, such as Au nanorods,[3,45] Au NPs,[46] upconverting NPs,[47] indocyanine,[48] black phosphorus,[49] azobenzene NPs,[50] cyanine dye,[51] and so forth, have been used to trigger the release of biomolecular cargos encapsulated within NPs through light-induced hyperthermia, further resulting in significant anticancer effects. Nevertheless, their complicated fabrication processes, nonbiodegradability, and unstable property severely limited their further clinical applications. As a drug/gene carrier, the biocompatible GQDs with a planar structure are expected to overcome these limitations. GQDs exhibit a unique optical character of having a special absorption peak in the UV−visible light region. The heat generated from the light energy through GQD conversion can be utilized to perform PTT or trigger the release of the loaded therapeutic agents.

Herein, we reported a synergistic treatment strategy of pancreatic cancer using BCPV-functionalized GQDs as a

DOI: 10.1021/acsami.8b16168
ACS Appl. Mater. Interfaces 2019, 11, 2768−2781

Scheme 1. Schematic Illustration of the Synthesis of GQD/DOX/BCPV/siRNA Nanocomplexes as a Light-Triggered Payload Release System for Pancreatic Cancer Synergistic Therapy

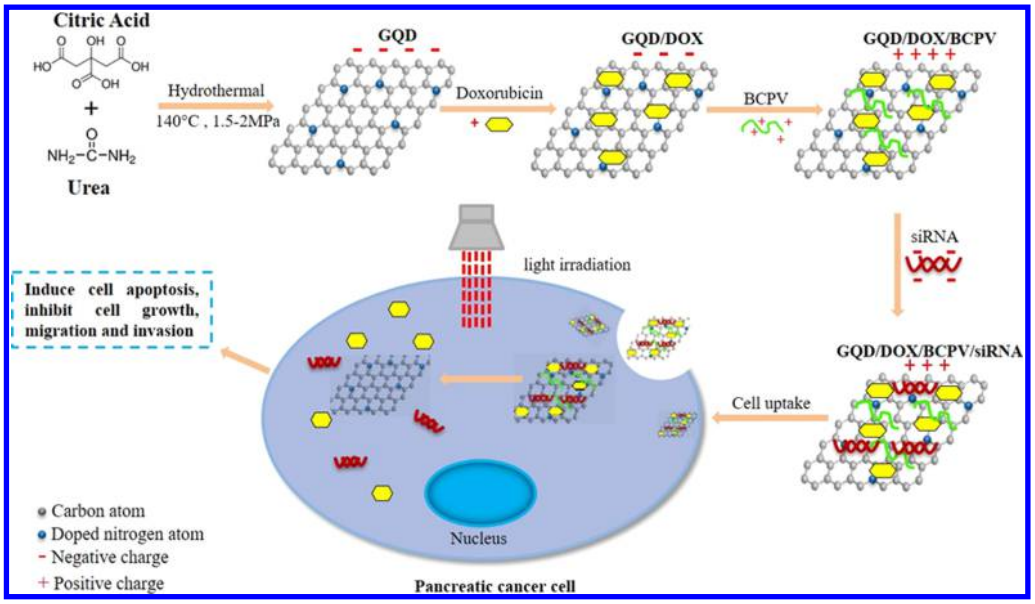

multifunctional platform for co-delivery drug and siRNA (Scheme 1). Negatively charged nitrogen-doped GQDs were successfully synthesized through a hydrothermal method with citric acid as the precursor and urea as the nitrogen source. Well-defined BCPVs were synthesized by ring-open polymerization (ROP) and thiol−ene functionalization. The tertiary amine groups grafted onto the biodegradable polylactide backbone endowed BCPVs with a positively charged property. Sequentially, in a step-by-step manner, GQDs were functionalized with DOX, BCPV, and siRNA to form a multifunctional co-delivery system. The delivery efficiency of DOX and siRNA by GQDs was evaluated on a pancreatic cancer cell line. Under laser irradiation, the cytosolic release of DOX and siRNA was enhanced, the K-ras gene expression was largely inhibited, and the synergistic anticancer effects were systematically evaluated and discussed.

2. EXPERIMENTAL SECTION

2.1. Synthesis and Characterization of Nitrogen-Doped GQD. The nitrogen-doped GQDs were synthesized using a hydrothermal method described earlier,[29,30,32] using citric acid as the precursor and urea as the nitrogen source. Briefly, 9 g of urea [$(NH_2)_2CO$, Sigma-Aldrich] and 6 g of citric acid ($C_6H_8O_7$, Sigma-Aldrich) were dissolved in 100 mL of ultrapure water at room temperature under stirring at 500 rpm for 5 min. The hydrothermal process was conducted in a stainless-steel autoclave with an inner Teflon liner for 4 h at a maintained temperature of 140 °C. The pressure of the autoclave was maintained at about 1.5−2.0 MPa during the whole duration of the hydrothermal process. To investigate the intrinsic structure, transmission electron microscopy (TEM, JEM-3000F, JEOL, Tokyo, Japan) was used. The optical properties of the GQDs were analyzed using a Shimadzu UV-2450 spectrophotometer and a Fluorolog-3 spectrofluorometer (Edison, NJ, USA), obtaining absorption and PL spectra, respectively. The zeta potential of the particles was measured using a Brookhaven 90Plus (Brookhaven Instruments Corporation).

2.2. Synthesis and Characterization of BCPVs. To prepare BCPVs, a precursor of allyl functional polylactides (APLAs) needs to be first synthesized via ROP. Briefly, allyl functional lactide (ALA, 800 mg; 4.7 mmol; 35 equiv), lactide (LA; 676 mg; 4.7 mmol; 35 equiv), benzyl alcohol (BnOH; 14.5 mg; 0.134 mmol; 1 equiv), and 4-dimethylaminopyridine (65.3 mg; 0.536 mmol; 4 equiv) were introduced to a 10 mL polymerization flask, followed by adding 2 mL of dry dichloromethane. Sequentially, the temperature of the flask was controlled at 35 °C using an oil bath. The polymerization reaction time was controlled for 7 days, at which the conversion of the ALA and LA monomers reached higher than 90%. After the reaction, the resulting products were precipitated from cold methanol to remove the unreacted monomers and catalysts, followed by the analysis of ^{1}H nuclear magnetic resonance (NMR). The ^{1}H NMR result indicated that the APLA had a molecular structure of poly$(ALA_{0.43}$-*co*-$LA_{0.57})_{64}$. Subsequently, the APLA was converted to BCPVs through thiol−ene click functionalization. First, poly$(ALA_{0.43}$-*co*-$LA_{0.57})_{67}$ (100 mg; $[ene]_0$ = 0.277 mmol; 1 equiv), 2-(diethylamino)ethanethiol hydrochloride (140 mg; $[SH]_0$ = 0.831 mmol; 3 equiv), and 2,2′-dimethoxy-2-phenylacetophenone (28.2 mg; 0.110 mmol; 0.4 equiv) were introduced in a 10 mL reaction flask, followed by adding 3 mL of chloroform to dissolve all the reactant. Such reactant feeding amount led to the molar ratio of $[ene]_0/[SH]_0$ being equal to 1:3 in the reaction. Then, the flask was exposed to UV light (wavelength λ_{max} = 365 nm; 6 W; 0.12 A) for 30 min. After the UV irradiation, the resultants were dialyzed against acetone (MW cut-off: 3.5 kDa) to remove any unwanted impurities. After the dialysis, BCPVs were obtained and characterized by ^{1}H NMR to acquire their charge density. The result showed that the BCPV had a charge density of 33% relative to the PLA backbone.

2.3. Conjugation and Characterization of GQD/DOX/BCPV/siRNA Nanocomplexes. There are three stages of conjugation in the formation of the GQD/DOX/BCPV/siRNA nanocomplexes. In the first stage, GQDs were mixed with DOX for 24 h. Next, the GQD/DOX nanocomplexes were dialyzed against ultrapure deionized (DI) water for 48 h. The loading efficiencies of the GQD/DOX were determined by measuring the absorbance of the GQD/DOX nanocomplexes followed by comparing the obtained absorbance spectra with the characteristic absorbance spectra of GQDs and DOX. In the second stage, the dialyzed GQD/DOX nanocomplexes were mixed with BCPV at different weight ratios for 1 h. In the last stage of conjugation, different weight ratios of GQD/DOX/BCPV and siRNA were mixed for 30 min before being analyzed using agarose gel electrophoresis. The zeta potential of different formulations was analyzed using a Brookhaven 90Plus (Brookhaven Instruments Corporation, Holtsville, NY, USA), whereas the particle size of the GQD/DOX/BCPV/siRNA nanocomplexes were observed using TEM (JEOL USA, Inc., Peabody, MA, USA).

DOI: 10.1021/acsami.8b16168
ACS Appl. Mater. Interfaces 2019, 11, 2768−2781

2.4. Cell Culture. Human cancer cell lines, MiaPaCa-2 (pancreatic cancer cell line), PANC-1 (pancreatic cancer cell line), A549 (lung cancer line), and HepG2 (hepatocellular carcinoma cell line), obtained from American Type Culture Collection were used in this study. The cells were grown in culture with Dulbecco's modified Eagle's medium (DMEM, HyClone), supplemented with 10% fetal bovine serum (FBS, HyClone), 100 units/mL of penicillin (Gibco), and 100 μg/mL of streptomycin (Gibco) with a 37 °C under humidified atmosphere containing 5% carbon dioxide as described previously.[10]

2.5. Cell Cytotoxicity. According to our previous experience,[40,52] four different cell lines, namely, A549, HepG2, PANC-1, and MiaPaCa-2, were seeded in 96-well plates with a cell count of 5×10^3 per well, leaving them to adhere for 24 h. The cells were treated with different concentrations of GQDs or BCPVs for 48 h. The cell viability was measured using a 3-(4,5-dimethylthiazol-2-yl)-2,5-diphenyltetrazolium bromide (MTT) assay kit. Cell viability was obtained by normalizing the absorbance of the sample well against that from the BLANK well and was expressed in terms of percentage. The nontreated cells were assigned as 100% viability.

2.6. Cell Transfection. A custom-synthesized K-ras siRNA^{FAM} was purchased from Shanghai GenePharma Co., Ltd. (Shanghai, P. R. China). The sense and antisense sequences were as follows—sense: 5′-GUUGGAGCUUGUGGCGUAGUU-3′; antisense: 5′-CUACGCCACAAGCUCCACUU-3. MiaPaCa-1 cells were seeded in six-well plates in DMEM with 10% FBS to give 30−50% confluence at the time of transfection. siRNAs were mixed with GQD/DOX/BCPV nanocomplexes with a gentle vortex and left to rest for 1 h. Then, the above GQD/DOX/BCPV/siRNA nanocomplexes were added into the six-well plates and left for incubation for 4 h. After that, some of the cells were imaged using an inverted fluorescence microscope (Nikon Eclipse-Ti). Naked GQDs, GQD/BCPV, DOX, GQD/DOX/BCPV, and GQD/BCPV/siRNA^{FAM} were used in a separate parallel experiment at the same dosage level. Gene expression was monitored using quantitative real-time polymerase chain reaction (PCR) at 48 h post transfection and western blot at 72 h post transfection.

2.7. Fluorescence Imaging. A Nikon Eclipse-Ti inverted microscope was used to capture in vitro fluorescence images. After 4 h of incubation with GQD/DOX/BCPV/siRNA^{FAM} nanocomplexes, the transfected cells were washed thrice with phosphate-buffered solution (PBS) followed by fixation with 4% formaldehyde. Subsequently, the cells were stained with 4′,6-diamidino-2-phenylindole (DAPI, Sigma) for nuclear counterstaining. The filter for the inverted microscope was set for GQDs (excitation at 405 nm and the emission was collected with a 450/50 nm band pass filter), FAM (carboxyfluorescein, excited with a 488 nm laser and the emission was collected with a 525/50 nm band pass filter), and DOX (excited with 540 nm and emission was collected with a band pass filter 605/50 nm). Fluorescence intensity was determined using a FACSCalibur flow cytometer (Becton Dickinson, Mississauga, CA). The cells were first washed with PBS thrice before harvested by trypsinization. To quantify the fluorescence intensity, GQD, FAM, and DOX served as the luminescent markers with a filter set, respectively, for Buv395, fluorescein isothiocyanate (FITC), and phycoerythrin to collect fluorescence signals.

2.8. Analysis of Gene Transcription. After the cells were transfected for 48 h, the transcription level of K-ras gene was investigated according to our previous experience.[53] In detail, the total RNA was extracted from MiaPaCa-2 cells using a TRIzol reagent (Invitrogen) and quantified using a micro-spectrophotometer (NanoDrop ND-1000). Total RNA (2 μg) was reverse-transcribed to complementary deoxyribonucleic acid (DNA) using a reverse transcriptase kit from Promega in accordance with manufacturer's instructions. The mRNA level of K-ras gene was measured by real-time PCR using a SYBR green dye (Promega) in an ABI PRISM 7500 applied biosystem normalized to the expression of glyceraldehyde-3-phosphate dehydrogenase (GAPDH). The primer sequences were as follows: K-ras: 5′-AGAGTGCCTTGACGATACAGC-3′ (sense), 5′-ACAAAGAAAGCCCTCCCCAGT-3′ (antisense); GAPDH: 5′-ACCACAGTCCATGCCATCAC-3′ (sense), GAPDH 5′-TCCACCACCCTGTTGCTGTA-3′ (antisense).

2.9. Western Blotting. MiaPaCa-2 cells were first seeded in six-well plates followed by transfection with GQD/DOX/BCPV/siRNA nanocomplexes for 72 h. Prior to the isolation of protein, the cells were washed twice with PBS and harvested using lysis buffer (50 mM Tris-HCl pH 7.4, 150 mM NaCl, 1 mM ethylenediaminetetraacetic acid, and 1% Triton X-100). The total isolated protein concentration was determined using a microspectrophotometer (NanoDrop ND-2000). Denatured cellular extracts (5 μg) were resolved by 10% Tris-glycine sodium dodecyl sulfate −polyacrylamide gels using the Mini-Sub Cell GT system (Bio-Rad, CA). Protein bands in the gel were then transferred to nitrocellulose blotting membranes. Membranes were incubated for overnight at 4 °C followed by washing with buffer (1× PBS, 0.05% Tween 20) and 3% nonfat milk and then incubated for 4 h with the primary rat antihuman K-ras antibody (Abcam) or antihuman GAPDH antibody (Abcam). The membranes were washed with PBS/Tween 20 and then horseradish peroxidase-labeled antirat secondary antibody was used for secondary incubation for 1 h at room temperature. K-ras and GAPDH proteins were then visualized with chemiluminescent substrate (ECL detection reagent, Sigma-Aldrich, USA) by the enhanced chemiluminescence system.

2.10. Assays of Cell Proliferation, Migration, and Invasion. The anticancer effect of GQD/DOX/BCPV/siRNA nanocomplexes on proliferation of MiaPaCa-2 was determined by the MTT assay as described above. The therapeutic effect on cell migration was determined using the wound-healing assay. Briefly, 1×10^4 of MiaPaCa-2 cells were seeded in 24-well plates followed by transfection with GQD/DOX/BCPV/siRNA nanocomplexes for 48 h, in which the cells almost achieve confluence. Then, a scratch wound was created on the surface containing the cells using a sterile pipette tip. The cells were continually incubated for 48 h in a complete culture medium, and then the cells were imaged using an inverted fluorescence microscope. The rate of wound healing was determined by evaluating the distance of migration in the scratch wound at 0 and 48 h (0 h is the time of scratching). NIS-Elements Br Analysis 4.0 software was used to analyze the migration distance. The invasive capability of the MiaPaCa-2 cells transfected with GQD/DOX/BCPV/siRNA nanocomplexes was determined using an 8.0 μm BD BioCoat Matrigel invasion chamber assay system (BD Biosciences) according to manufacturer's protocol with minute modifications. Concisely, GQD/DOX/BCPV/siRNA nanocomplex-transfected MiaPaca-2 cells were seeded in the upper chamber which contained FBS-free medium. The bottom chamber was filled with 10% FBS medium, which served as a chemoattractant. The cells were incubated for further 48 h. Next, the cells in the upper chamber were removed with swabs followed by staining the cells of piercing the Matrigel matrix membrane with Giemsa staining in PBS for 5 min. The number of invaded cells were viewed and counted under the microscope in five random views.

2.11. Apoptosis Assays and Cell Colony Formation. The apoptosis rate of the transfected cells was determined using an FITC Annexin V Apoptosis Detection Kit I (BD Pharmingen) according to manufacturer's protocol. Annexin V is widely used as an early apoptosis indicator as it has a strong affinity to phospholipid phosphatidylserine of the cell membrane, which is widely available in the exterior membrane of apoptotic cells. Propidium iodide (PI) is a type of dye to identify the cells with a ruptured membrane and is commonly used to classify dead and damaged cells. In short, 1×10^6 MiaPaCa-2 cells were seeded in a six-well plate, followed by transfection with GQD/DOX/BCPV/siRNA nanocomplexes for 72 h. The cells were then collected and washed twice with cold PBS and suspended in binding buffer. Then, flow cytometry analysis was used to determine the apoptotic cells. Cell colony formation assay is a high-throughput tool for drug screening to reduce animal testing. Hence, we assessed the therapeutic effect of different formulations by cell colony formation assay according to previous reports with minor modifications.[8,54,55] Briefly, 500 single viable MiaPaCa-2 cells were mixed with 0.3% low melting point agarose gel (containing 10% FBS), and then the cells were plated in 35 mm Petri dishes that were

DOI: 10.1021/acsami.8b16168
ACS Appl. Mater. Interfaces 2019, 11, 2768−2781

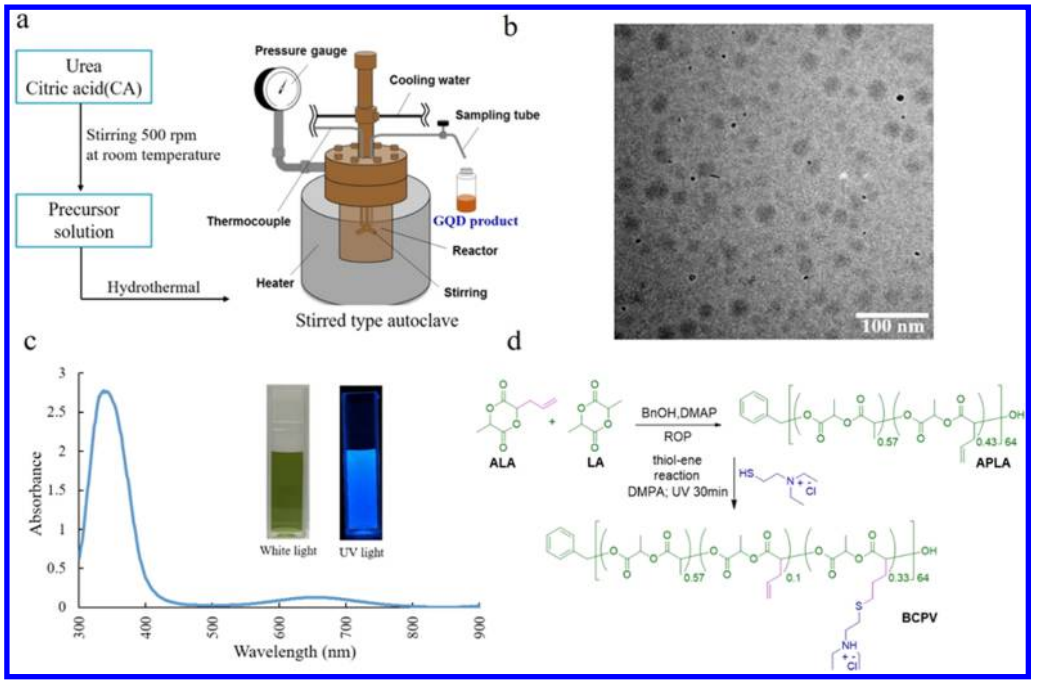

Figure 1. (a) GQDs were synthesized via a hydrothermal method using urea and citric acid as synthetic source. (b) TEM image of naked GQDs. (c) Absorption spectra of naked GQDs was analyzed by a spectrophotometer. The inset shows naked GQDs solvent (1 mg/mL) under white light or UV illumination. (d) Positive-charged polymer, BCPV, was synthesized via ROP and thiol−ene functionalization.

precoated with 0.6% low melting point agarose gel (containing 10% FBS). The cells were then incubated for one week to form colonies. After that, the cells were treated with different formulations, and the sizes of formatted colonies were measured under a microscope.

2.12. Light-Triggered DOX and siRNA Release from Nanocomplexes. MiaPaCa-2 cells were seeded in a six-well plate with a density of 1×10^5 cells per well with DMEM, subsequently followed by transfection with GQD/DOX/BCPV/siRNA for 4 h. Before illumination, the treated cells were rinsed thrice with PBS buffer to remove any free nanocomplexes. A multimode fiber-coupled diode laser with a center wavelength of 650 nm and 0.22 numerical aperture with a straight cleaved fiber end was used to irradiate the cells with laser light. The output power was adjusted to achieve different power densities. The duration of irradiation was fixed at 15 min. The fluorescence intensity from the cells was determined using flow cytometry. After irradiation, the cell bioactivity was evaluated by an MTT assay and an apoptosis kit.

2.13. Statistical Analysis. The data are presented as mean ± standard deviation (SD). Statistical analysis was performed using analysis of variance. All statistical calculations were performed with the SPSS 11.0 software package. When two comparisons were obtained, Student's unpaired two-tailed *t*-test was used. A *P* value less than 0.01 is regarded as statistically significant.

3. RESULTS AND DISCUSSION

3.1. Synthesis of GQDs and BCPV. GQDs were synthesized using hydrothermal reaction of citric acid and urea with ultrapure water as the solvent (Figure 1a).[29] High-resolution TEM results showed that the naked GQDs had an average particle size of 23 ± 3.2 nm (Figure 1b). The absorption spectrum of the prepared GQDs was investigated using UV−vis spectroscopy, and GQDs exhibited a major absorption peak at 365 nm and a minor absorption peak at 650 nm (Figure 1c). The emitted blue luminescence can be viewed under UV lamp illumination (Figure 1c inset). The synthesized GQDs show an excitation wavelength-dependent photoluminescence, and the most intense fluorescence appears at 440 nm upon 300 nm excitation (Figure S1). According to our previous reports, the biodegradable charged polymer, BCPV, was synthesized via ROP and thiol−ene functionalization (Figure 1d).[38,56] The final chemical structure of BCPV was characterized using ^{1}H NMR (Figure S2). The presence of tertiary amine-based cationic groups in the polymer backbone endowed BCPV with a high positive-charged potential of 62 ± 2.2 mV. As a gene or a drug carrier, the biotoxicity of components is the main limited factor in practical application. Prior to further applications, the intrinsic cytotoxicity of GQDs and BCPV was first evaluated on four different cell lines via MTT assay. After 48 h post incubation, the results in Figure S3 showed that all cells still possessed over 90% viability even at dosages of up to 4 mg/mL of GQDs and 160 μg/mL of BCPV, respectively. These results clearly suggested that both GQDs and BCPV are highly biocompatible and noncytotoxic over a large dosage range.

3.2. Formation and Characterization of BCPV-Coated GQD Nanocomplexes. For the efficient loading of biomolecules, it is important to optimize the weight ratios among GQDs, DOX, BCPV, and siRNA as well as the sequence of the conjugation order. First, to determine the amount of conjugated DOX on the GQDs, two calibration curves with varying concentrations of GQDs and DOX were first prepared (Figure S4a,b). GQDs were mixed with DOX for 24 h before dialyzing it against DI water, resulting in the formation of GQD/DOX nanocomplexes. Subsequently, the absorbance spectra of GQD/DOX nanocomplexes were measured. It was calculated that 1 mg of GQD was capable of loading 1.6 μg of DOX (Figure S4c). The negatively charged surface of GQD/DOX nanocomplexes allowed positively charged BCPV to be subsequently conjugated via electrostatic interaction, resulting in GQD/DOX/BCPV nanocomplexes. It was observed that when applying an electric field, the naked GQDs with a negative charge in the sample wells will run into the positive electrode. When the amount of coated BCPV on the GQD/DOX steadily increased, the running direction of the

DOI: 10.1021/acsami.8b16168
ACS Appl. Mater. Interfaces 2019, 11, 2768−2781

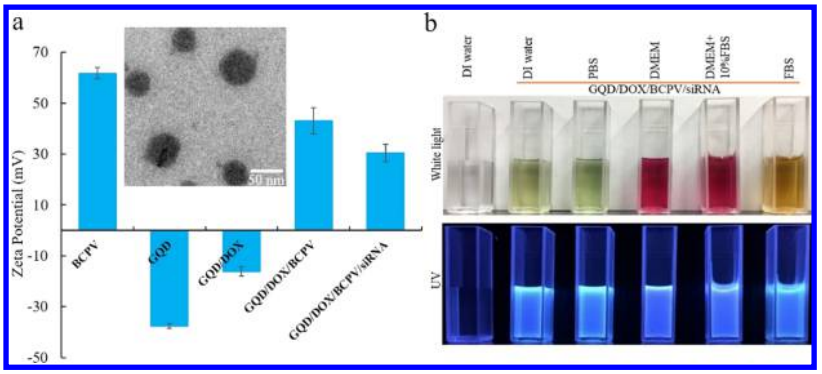

Figure 2. (a) Changed profiles of zeta potential were analyzed by DLS after step-by-step functionalization of naked GQDs with DOX, BCPV, and siRNA. TEM image of the fabricated GQD/DOX/BCPV/siRNA nanocomplexes (inset), scale bar: 50 nm. (b) GQD/DOX/BCPV/siRNA nanocomplexes were dispersed in different physiological solutions for 48 h. The dissolved status and fluorescence of GQD/DOX/BCPV/siRNA nanocomplexes were observed under white light and UV illumination, respectively.

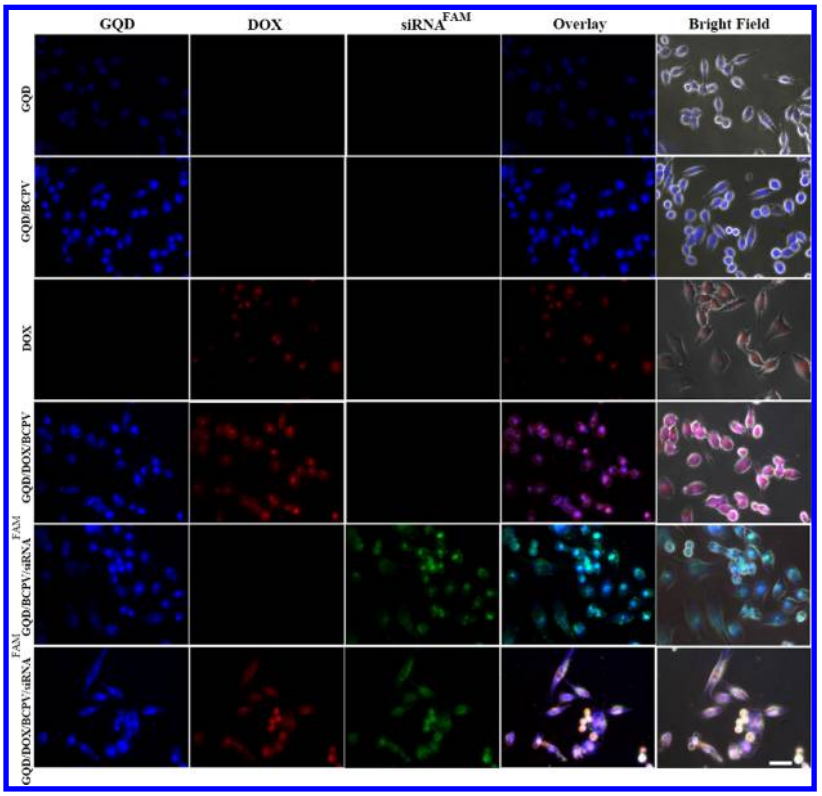

Figure 3. Fluorescence microscopy images of MiaPaCa-2 cells treated with different formulations for 6 h. The blue fluorescence originates from GQDs while the red fluorescence originates from DOX. The fluorescence originates from the FAM-labeled siRNA is rendered in green. For the GQD/DOX/BCPV/siRNA-treated group, according to the preoptimized weight ratio, the final concentration of GQDs was fixed at 1 mg/mL, DOX was fixed at 1.6 μg/mL, BCPV was fixed at 120 μg/mL, and siRNA was fixed at 4 μg/mL, and these concentrations are all used in the following cell-related experiments. Scar bar: 10 μm.

resulting GQDs was reversed to the negative electrode (Figure S5a). It was found that the optimized weight ratio of BCPV and GQD/DOX is at 0.12:1 as all the GQDs (with a zeta potential of 43 ± 5.1 mV) migrated toward the negative electrode in the electrophoresis agarose gel. The introduction of BCPV not only endowed the GQDs with biocompatibility and stability, but also rendered them with a positively charged character, which facilitated the resulting GQDs to interact with siRNA molecules and to be internalized by cancer cells.

The optimized GQD/DOX/BCPV nanocomplexes were then mixed with siRNA at different weight ratios, ranging from 150:1 to 500:1. Similarly, agarose gel electrophoresis was also used to determine the optimum weight ratio of siRNA and GQD/DOX/BCPV nanocomplexes. In this process, GelRed served as the indicator of siRNA. The un-loaded free siRNA will run into the positive electrode because of the electric attractive force. At the weight ratio of 250:1, it can be observed that most of the siRNA has been fully retarded in the sample wells (Figure S5b), which means most of the loaded siRNA molecules have been encapsulated in the GQD-based nanocomplexes. Hence, the prefabricated GQD/DOX/BCPV nanocomplexes were conjugated with siRNAs at the weight ratio of 250:1 to construct the GQD/DOX/BCPV/siRNA nanocomplexes. The change profiles of zeta potential in the fabricated process were monitored by dynamic light scattering (DLS) measurements. The results indicated that the final

DOI: 10.1021/acsami.8b16168
ACS Appl. Mater. Interfaces 2019, 11, 2768−2781

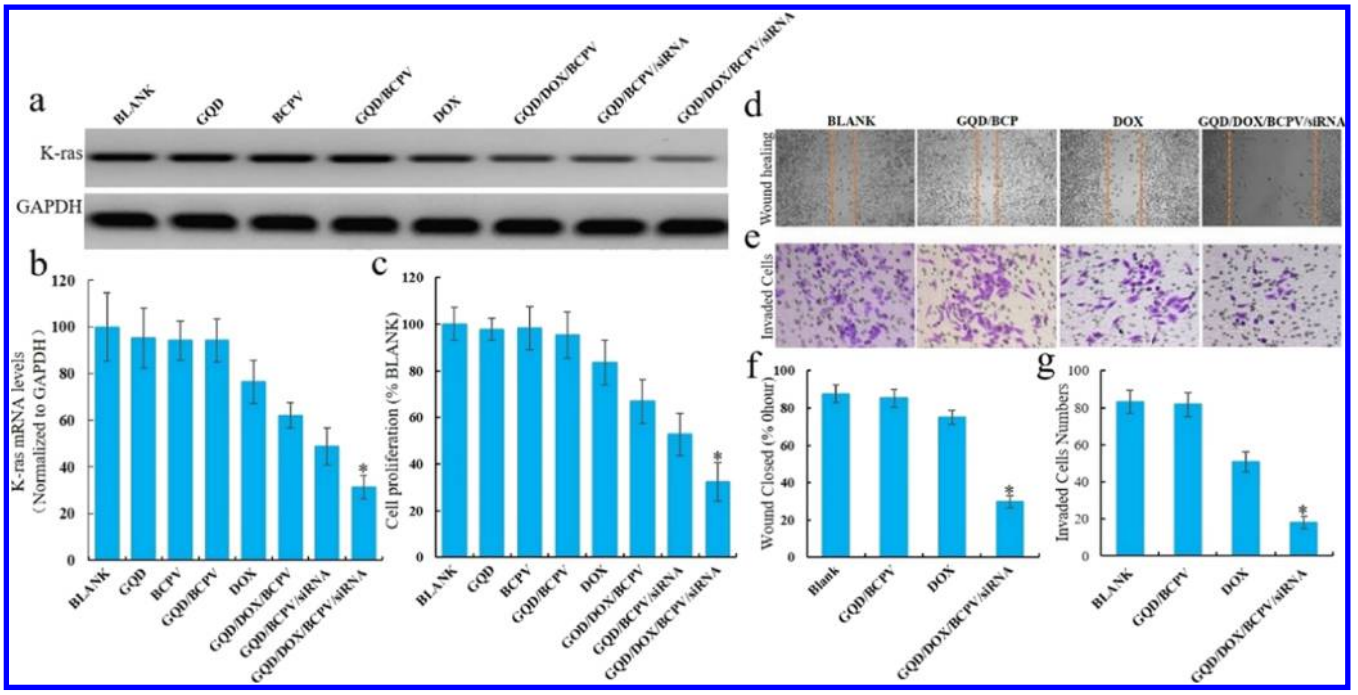

Figure 4. (a) Cell groups were treated with different formulations for 48 h, and the relative protein expression of K-ras in the treated MiaPaCa-2 cell was detected by western blot. GAPDH was used as the intra reference for protein quantification. (b) Gene transcription level of K-ras was evaluated by real-time reverse transcription PCR assay. (c) Cell proliferation was evaluated via MTT assay. (d,f) After treated with different formulations for 48 h, the cell migration was evaluated by wound-healing assay. Quantitative evaluation on the percentage of the wound window closed after treatment, values were normalized by the initial wound window width. (e,g) Cell invasion was evaluated by trans-well chamber model. The invaded cells penetrated through the Matrigel-coated membrane in the trans-well chamber. The invaded cells were stained with Giemsa and were counted in the random macroscopic field (20× magnification). Results are represented as mean ± SD, $n = 6$; *, $P < 0.01$, compared with other groups.

GQD/DOX/BCPV/siRNA nanocomplexes have a positively charged surface charge of 30 ± 3.4 mV (Figure 2a). The TEM image indicated that the final nanocomplexes had a diameter of 65 ± 5.3 nm (Figure 2a inset). These characteristics of nanocomplexes were expected to benefit the interaction of nanocomplexes with the negative-charged cell membrane, thus facilitate cell uptake. Such results also suggested that well-defined GQD/DOX/BCPV/siRNA nanocomplexes can be prepared by only using electrostatic interactions under the designed conjugation order. Such preparation methodology is facile and efficient, thereby benefiting the subsequent large-scale production of the new delivery system.

To investigate the photostability and chemical stability of GQD/DOX/BCPV/siRNA nanocomplexes with the optimized component ratio and conjugation sequence, the nanocomplexes were dispersed in four different physiological solutions such as PBS, DMEM, DMEM + 10% FBS, and 70% FBS. After 48 h of co-incubation, no significant fluorescence quenching and aggregation of the nanocomplexes were observed, demonstrating the high colloidal stability of the nanocomplexes in various biological solutions (Figure 2b). The stability of therapeutic delivery systems in photo and chemical activities strongly influences their delivery and therapeutic efficiencies. With high photo/chemical stability, the delivery systems are capable of retaining their designed biomedical functions after reaching the objective destinations such as targeted tumor tissues.[57,58]

3.3. Delivery Efficiency of DOX and siRNA. To demonstrate the transfection efficiency of GQD/DOX/BCPV/siRNA^{FAM} nanocomplexes, MiaPaCa-2 cells, a pancreatic cancer cell line, were treated with different formulations for 4 h, including naked GQDs, GQD/BCPV, DOX, GQD/DOX/BCPV, GQD/DOX/siRNA^{FAM}, and GQD/DOX/BCPV/siRNA^{FAM}. For indicating the transfection efficiency of siRNA, the used siRNAs were labeled by FAM fluorescein. After treatment, the cells were observed under an inverted fluorescence microscope. Figure 3 shows fluorescent signals from GQDs (blue color), DOX (red color), and siRNA^{FAM} (green color) in MiaPaCa-2 cells. It was clearly observed that the uptake amount of GQDs was significantly enhanced after the BCPV modification. This is due to the property change of the surface charge of GQD/BCPV nanocomplexes from negative (naked GQD) to positive as positively charged nanocomplexes would easily penetrate into the negatively charged cell membrane.[59] Meanwhile, the fluorescence intensities of intracellular DOX and siRNA were also significantly increased when BCPV-modified GQDs were used as the nanocarrier, suggesting that the coating of BCPV is beneficial for enhancing the cellular uptake efficiencies of DOX and siRNA. The DOX and siRNA fluorescence signals overlapped well with the fluorescence from the GQDs, which clearly verifies that the GQDs can serve as a nanocarrier for the co-delivery of DOX and siRNA into cells. The fluorescence signal from the GQDs could render intracellular tracking capability and offer possibility for image-guided drug delivery.

Flow cytometry was further employed to quantify the transfection efficiencies of DOX and siRNA^{FAM} in GQD/DOX/BCPV/siRNA^{FAM} nanocomplex-treated cells. Results indicated that the cells treated with GQD/DOX/BCPV/siRNA^{FAM} nanocomplexes present both strong fluorescence intensities of DOX and FAM (Figure S6). The corresponding fluorescence intensities from GQD/DOX/BCPV/siRNA^{FAM}

DOI: 10.1021/acsami.8b16168
ACS Appl. Mater. Interfaces 2019, 11, 2768−2781

nanocomplex-treated cells were evaluated to be 3477 a.u (DOX) and 1806 a.u (FAM), which are much higher than those of the cells treated with free DOX and naked siRNA. Moreover, there is only a negligible difference between the DOX fluorescence intensities from GQD/DOX/BCPV (3425 a.u) and GQD/DOX/BCPV/siRNA (3477 a.u) nanocomplex-treated tumor cells. These flow cytometry results are consistent with the previous cell fluorescence imaging results and further demonstrated that GQD-based carriers can effectively co-deliver DOX and siRNA into pancreatic cancer cells.

3.4. Gene Knockdown Efficacy of GQD/DOX/BCPV/siRNA Nanocomplexes. To verify the knockdown efficiency of GQD/DOX/BCPV/siRNA nanocomplexes, the expression of the mutated K-ras gene was respectively quantified at the mRNA level by real-time PCR and at the protein level by western blot. By using GAPDH gene as the reference, the protein and mRNA levels of K-ras gene in different treated groups were measured and normalized to the BLANK group. Results indicated that the cells treated with GQDs, BCPV, DOX, and GQD/BCPV formulations showed no significant difference in both protein (Figure 4a) and mRNA (Figure 4b) levels of the mutated K-ras gene as compared with the BLANK group. On the other hand, in the GQD/DOX/BCPV/siRNA nanocomplex-treated cells, the expression of K-ras gene was significantly suppressed when compared to the other nanocomplex-treated groups. Thus, these results clearly suggest that the co-delivery of DOX and siRNA had a superior multiplied effect in downregulating K-ras gene expression of the pancreatic cancer cell line.

3.5. Synergistic Anticancer Efficacy of GQD/DOX/BCPV/siRNA Nanocomplexes. The K-ras gene, encoding a membrane-bound GTP-binding protein, is responsible in mediating various cellular functions such as cell proliferation, cell division, and angiogenesis.[60] The K-ras mutation was reported to promote cell metastasis, drug resistance, and antiapoptosis through multiple cell signaling pathways, eventually causing cancer formation.[8] DOX, as a chemotherapeutic drug, functions by binding to DNA-associated topoisomerase enzymes II and thus induces a range of cytotoxic effects. On the basis of the mechanism, DOX is therefore capable of blocking tumor cell growth and proliferation.[61] In this study, the treatment effects of GQD/DOX/BCPV/siRNA nanocomplexes on pancreatic cancer were systematically evaluated. The ability of the nanocomplexes on inhibiting the growth of MiaPaCa-2 cells was assessed by MTT assay. Figure 4c shows that the co-delivery of DOX and siRNA into the cells via GQD/DOX/BCPV/siRNA nanocomplexes remarkably reduced the cell proliferation by 67 ± 8.2% compared with the BLANK group. It is worth noting that GQD/DOX/BCPV/siRNA-treated groups yield much more robust cell-killing effect than GQD/DOX/BCPV-treated groups, mainly attributed to the siRNA-regulated down-regulation of mutant K-ras gene. Meanwhile, the amount of apoptotic cells of the treated MiaPaCa-2 cells was further evaluated by FITC-labeled annexin V and PI staining assay. Results indicated that the cell group treated with GQD/DOX/BCPV/siRNA nanocomplexes exhibited the highest percentage of apoptotic cell population (28 ± 1.9%) as compared to the BLANK (2.5 ± 0.6%), GQD/BCPV (2.3 ± 0.5%), and DOX (10.3 ± 1.9%) groups (Figure S7). The enhanced therapeutic effect was attributed to the strong synergism between K-ras siRNA and DOX. K-ras protein is a key regulation of antiapoptotic cellular defense to prevent cell apoptosis by activating the survival signal in pancreatic cancer cells. Therefore, the suppression of mutant K-ras gene expression via siRNA can both increase the cell sensitivity to chemotherapeutics and promote DOX-induced cell apoptosis for enhanced chemotherapy. Such results implied that the silencing expression of the antiapoptotic K-ras protein via siRNA successfully elevated cytotoxicity of DOX and induced more apoptotic cells in the treated cells.

Metastasis is the primary cause of death in pancreatic cancer patients. Metastasis involves a complicated multistep process that starts with the migration of primary cancer cells to the adjacent tissues.[7] Hence, the inhibition in cell migration and invasion is very important for combating pancreatic cancer. By creating a wound on the monolayer of MiaPaCa-2 cells, cell migration can be evaluated by monitoring the width of the wound after treatment with different formulations (Figure 4d,f). In the nontreated blank group, a decrease of the wound window width was clearly observed after 48 h of incubation. The cells started to migrate to the open space in-between the wound margins and the wound boundaries became cluttered. Similar phenomena were also observed in GQD/BCPV- and DOX-only treated groups. In comparison with the control groups, an obvious suppressed efficacy in wound healing was observed in GQD/DOX/BCPV/siRNA nanocomplex-treated group. Additionally, the invasion capability of MiaPaCa-2 cells was assessed using a Matrigel invasion chamber assay. As shown in Figure 4e,g, the invaded cell population in GQD/DOX/BCPV/siRNA-treated group was significantly reduced when compared with other formulation-treated groups. All these results suggest that the combination of gene-/chemo therapy via GQD/DOX/BCPV/siRNA nanocomplexes had an enhanced synergistic anticancer efficacy on inhibiting the migration and invasion abilities of pancreatic cancer cells. Such a feature of the nanocomplex carrier is very vital when metastasis encountered in cancer therapy.

3.6. Photothermal Property of GQD-Based Nanocomplexes. GQDs were synthesized by hydrothermal reaction of citric acid and urea with ultrapure water as the solvent. Urea played an important role in the near infrared absorbance properties of the GQDs. A high concentration of urea introduces a large number of pyrrolic nitrogen on the GQD surface, contributed to the photoluminescence and photothermal efficiency of the GQDs. The detailed optical mechanism of GQD has been interpreted elaborately in our previous report.[30] The synthesized GQDs in this study presented a special absorption peak at 650 nm. The photothermal property of the GQD-based nanocomplexes was evaluated under different power inputs with 650 nm laser irradiation. The temperature of the GQD/DOX/BCPV/siRNA nanocomplex solution (1 mg/mL) elevated rapidly with an increase of laser power and irradiation time (Figure 5a). Water vapor-caused droplets were observed in the cuvette wall as a result of heating through the photothermal effect of the GQDs (Figure 5b). Meanwhile, functionalization of the GQDs with DOX, BCPV, or siRNA does not influence the photothermal conversion efficiency of the GQDs (Figure S8). After giving irradiation of laser light to GQD/DOX/BCPV/siRNA nanocomplex-containing and physiologically mimicking solutions (0.2 W/cm^2, 15 min), it was observed that the temperature-increased profiles in the tested solutions were quite similar to the temperature-increased profile in DI water (Figure S9). This demonstrated the high stability of the photothermal property of GQD/DOX/BCPV/siRNA nano-

DOI: 10.1021/acsami.8b16168
ACS Appl. Mater. Interfaces 2019, 11, 2768−2781

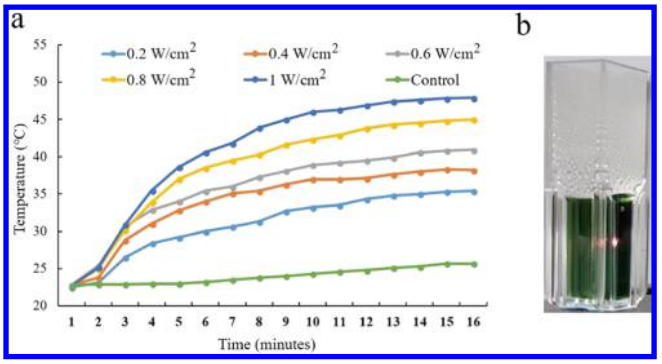

Figure 5. (a) Temperature-increased profile of the DI water solution from the photothermal effect of the GQD/DOX/BCPV/siRNA$^{K\text{-}ras}$ nanocomplexes (1 mg/mL) upon irradiation with a different power of 650 nm laser light for 15 min. (b) Water vapor-caused droplets were observed in the cuvette wall because of the evaporation from the photothermal effect of GQDs when irradiated with 1 W/cm^2 laser light.

complexes at different physiologically mimicking solutions and highlighted one of their unique biomedical merits as compared with other nanomaterial systems with a photothermal effect, in which quench problems may occur in various physiological environments.[4]

Moreover, the photothermal therapeutic effect of GQD/BCPV was investigated by exposing the treated cells to different laser light power inputs for 15 min. The cell viability was evaluated by MTT assay. It was observed that the inhibition efficiency of cell viability was enhanced when the laser power was gradually increased (Figure S10). These results demonstrated that the photothermal effect of the GQDs is laser dependent and PTT only occurred when the power of laser light exceeds 0.2 W/cm^2. The outstanding property of GQDs suggests its potential to be used as multifunctional nanocarriers for drug/gene delivery and cell imaging and as photothermal agents in cancer therapy.

3.7. Light-Triggered Payloads Release from GQD-Based Nanocomplexes. Under laser light irradiation, the GQDs were observed to be able to convert light energy into heat. Such heat may be further utilized to increase the mobility of the payloads of GQD/DOX/BCPV/siRNA nanocomplexes, thereby selectively releasing the payloads when the heat was generated from laser light irradiation.[46,51] To verify our thought, the GQDs were used to serve as a localized heat source to promote released DOX and siRNA of GQD/DOX/BCPV/siRNA nanocomplexes through photothermal effects under laser irradiation. To confirm that the therapeutic efficacy is only due to the light-triggered release of siRNA and DOX from the nanocomplexes, all the power of laser light in the following experiment was fixed at 0.2 W/cm^2. Under these conditions, the photothermal effect of GQD/DOX/BCPV/siRNA nanocomplexes on triggering the payload release can thus be clearly verified. Briefly, after the nanocomplex solution was irradiated with laser light at 650 nm for 15 min, the solution was centrifuged at 12 000 rpm for 10 min, and the fluorescence intensities of siRNA^{Cy3} and DOX in the supernatant were quantitatively measured by spectrophotometer at a 5 min interval. The release kinetic profile of siRNA and DOX from the nanocomplexes indicated a burst release of siRNA and DOX under the 650 nm laser light irradiation (0.2 W/cm^2, 15 min). The cumulative release amounts of siRNA and DOX from GQD/DOX/BCPV/siRNA nanocomplexes rapidly attained 80.8% and 63.73% at 15 min, respectively (Figure 6a,b). Without laser light irradiation, the cumulative release amounts of siRNA and DOX from GQD/DOX/

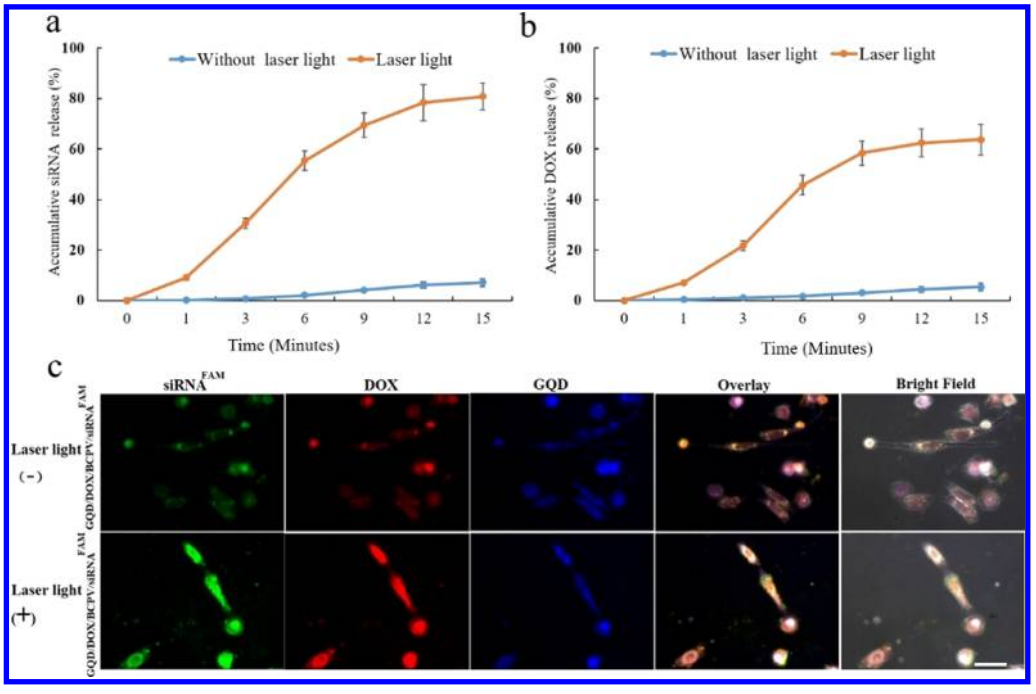

Figure 6. Release kinetic profile of siRNA^{FAM} (a) and DOX (b) in GQD/DOX/BCPV/siRNA^{FAM} nanocomplex solution under laser light irradiation (0.2 W/cm^2). (c) MiaPaCa-2 cells were first preincubated with GQD/DOX/BCPV/siRNA^{FAM} for 6 h and then cells were exposed to laser light irradiation (650 nm, 0.2 W/cm^2) for 15 min. The treated cells were observed under an inverted fluorescence microscope. The blue fluorescence from DAPI indicates the cell nucleus. The green fluorescence from FAM fluorescein indicates siRNA. The red fluorescence indicates the DOX distribution. Scar bar: 10 μm.

DOI: 10.1021/acsami.8b16168
ACS Appl. Mater. Interfaces 2019, 11, 2768−2781

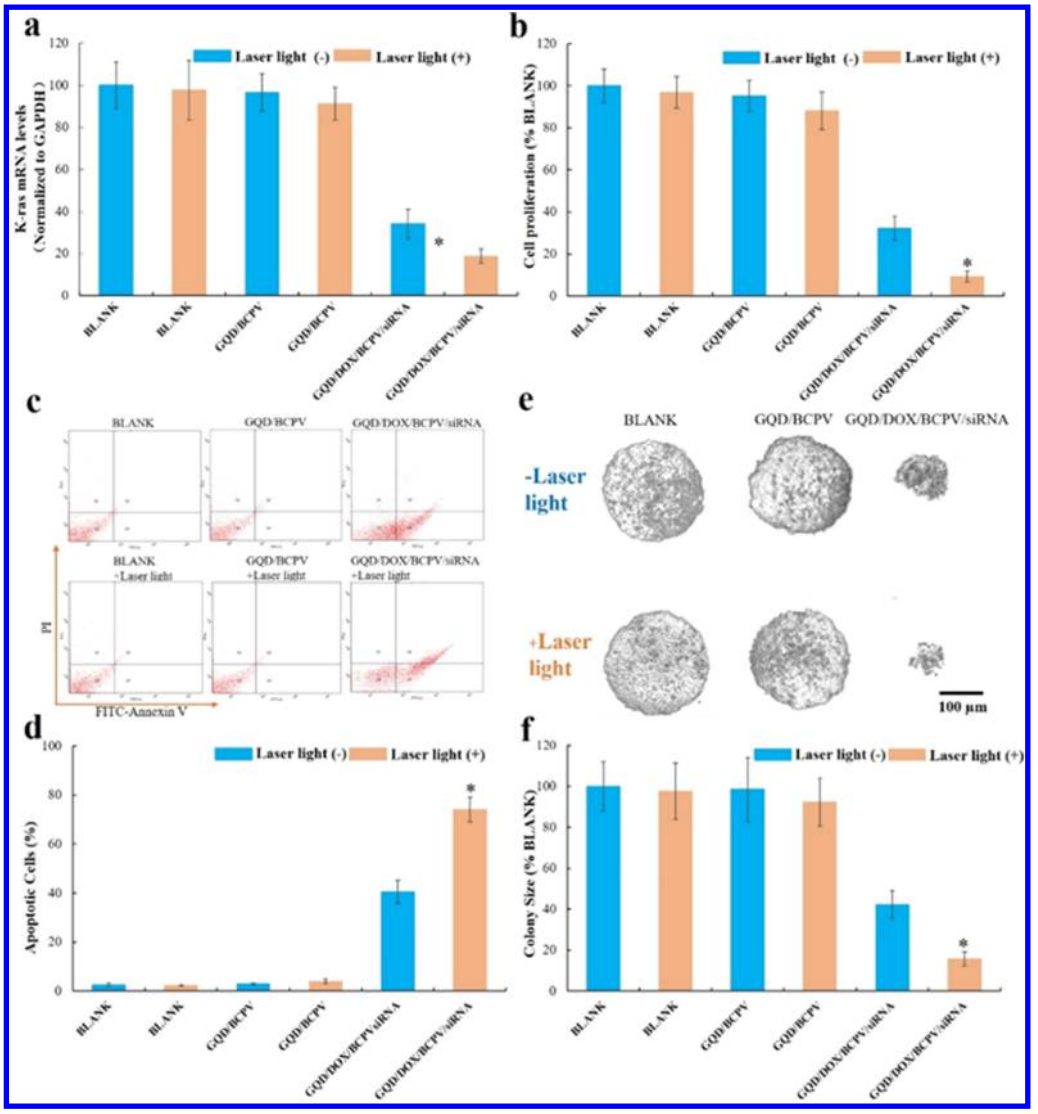

Figure 7. (a) MiaPaCa-2 cells were incubated with different formulations for 4 h and irradiated with laser (650 nm, 0.2 W/cm^2) for 15 min. After 48 h of continuous culture, the K-ras gene expression of MiaPaCa-2 cells was detected by real-time PCR assay. (b) Cell proliferation was evaluated by MTT assay. (C) After light irradiation, the apoptotic cells in different formulation-treated MiaCaPa-2 cells were assessed by FITC annexin V and PI co-stained. (d) Summary of the apoptotic rate of MiaPaCa-2 cells treated with different formulation after laser light irradiation. (e) Size and shape of MiaPaCa-2 cell colonies were observed under an inverted microscope. (f) Size summary of the formatted cell colony and normalized to the BLANK group. Results are represented as mean ± SD, n = 5; *, P < 0.01, compared with other groups.

BCPV/siRNA nanocomplexes, however, only had 7.21 and 5.43% at the same release time. Generating an efficient heat resource via laser irradiation, the GQDs therefore are capable of increasing the mobility of the payloads of the nanocomplexes and subsequently promoting the unpacking and dissociation of the payloads. Utilizing the photothermal effect, the GQD-based nanocarriers can thus be conferred with a triggered release function, which greatly increases the versatility of the resulting nanocarriers and largely enhances the therapeutic efficiency of the loaded payloads as well.

The therapeutic effect of the laser light-triggered siRNA/DOX release from GQD-based nanocomplexes was further investigated in vitro. First, MiaPaCa-2 cells were treated with GQD/DOX/BCPV/siRNA^{FAM} nanocomplexes for 4 h, in which siRNA was labeled with FAM fluorescein for displaying siRNA transfection. Subsequently, the pretreated cells were irradiated with laser light of 650 nm and 0.2 W/cm^2 for 15 min. The cell fluorescence images indicated that the laser-treated MiaPaCa-2 cells yielded higher fluorescence brightness originating from FAM and DOX when compared to the cells without laser irradiation (Figure 6c). Flow cytometry was further employed to quantitatively evaluate the light-triggered release of siRNA and DOX of GQD/DOX/BCPV/siRNA^{FAM} nanocomplexes intracellularly. Results indicated that, after irradiating the nanocomplex-treated cells by laser light, both the fluorescence intensities of FAM and DOX had significantly increased by 1.8 times and 2.2 times as compared with those resulting from the cells without laser irradiation (Figure S11). Overall, either the release study, the confocal observation, or the flow cytometry analysis corroborated that the laser light is capable of efficiently and rapidly triggering the loaded DOX and siRNA of the nanocomplexes in the treated MiaPaCa-2 cells. The developed GQD-based platform provides excellent time-resolved and spatially controlled intracellular release of drug and siRNA relying on laser light irradiation, suggesting multipotent function of nanocomplexes on cancer therapy.

DOI: 10.1021/acsami.8b16168
ACS Appl. Mater. Interfaces 2019, 11, 2768−2781

3.8. Light-Regulated Superior Anticancer Effect. After MiaPaCa-2 cells were treated with the nanocomplexes and exposed to the laser light, the K-ras gene knockdown efficiency of the nanocomplexes against MiaPaCa-2 cells was investigated by real-time PCR. It was observed that the laser light irradiation significantly enhanced the inhibition efficiency of the K-ras gene expression on the nanocomplex-treated MiaPaCa-2 cells (Figure 7a). Relative to the nanocomplexes without the laser light irradiation (K-ras expression level: 30.04%), the nanocomplexes with the laser light irradiation (K-ras expression level: 18.29%) had about 12% increase in K-ras gene downregulation efficiency, indicating that the controlled release of the siRNA from the nanocomplex via the laser light is quite vital for the loaded siRNA to accomplish its RNAi mechanism.

Moreover, the synergistic anticancer effect on MiaPaCa-2 cell was systematically evaluated. After laser light irradiation, the proliferation percentage of the MiaCaPa-2 cells treated by GQD/DOX/BCPV/siRNA nanocomplexes was reduced to 9.24% as compared to the blank control. Without laser light irradiation, GQD/DOX/BCPV/siRNA nanocomplex-treated groups, however, still exhibited a proliferation percentage value of 33% (Figure 7b). This result indicated that the laser light irradiation effectively triggered the rapid unpacking and release of their therapeutic payloads, thereby obviously enhancing the eventual therapeutic efficiency of DOX and siRNA in MiaCaPa-2 cells.

Moreover, it was also observed that the light irradiation enabled GQD/DOX/BCPV/siRNA nanocomplexes to result in more apoptotic MiaCaPa-2 cells. As shown in Figure 7c,d, without light irradiation, GQD/DOX/BCPV/siRNA nanocomplexes can only lead to 40.5 ± 4.65% cell apoptosis in the treated MiaPaCa-2 cells. However, after the light irradiation, the cell apoptosis resulting from the nanocomplexes significantly increased to 74.1 ± 4.98%. Such results indicated that the controlled and intracellular unpacking of the therapeutic agents from the nanocomplexes via laser irradiation effectively facilitated the interactions of the loaded agents and MiaPaCa-2 cells, thereby leading to higher apoptosis efficiency.

Furthermore, a cell colony formation assay was utilized to preliminarily evaluate the tumor inhibition efficiency of GQD/DOX/BCPV/siRNA nanocomplexes. The assay was reported to provide excellent environmental mimicking conditions to real tumor cells.[9,62] Because of the excellent mimicking conditions for in vivo tumor cell growth, the assay has been widely used to assess the antitumor activity of various types of cancer therapies.[62,63] In the assay, MiaPaCa-2 cells were first incubated for 1 week to form colonies. Afterward, the cells were treated with GQD/DOX/BCPV/siRNA nanocomplexes for 24 h, followed by laser light irradiation (0.2 W/cm^2, 650 nm, 15 min). The cells were then continuously incubated for another 1 week. Eventually, the final formed cell colonies were observed using an inverted microscope.

In Figure 7e,f, as compared with the control groups (BLANK and GQD/BCPV), the sizes of the nanocomplex-treated MiaPaCa-2 cell colonies were obviously reduced. With laser light irradiation, the nanocomplexes were capable of further diminishing the cell colony size. Moreover, the cell colonies failed to form a complete and spheroid-like aggregate. The results revealed that the reduced MiaPaCa-2 cell activity resulting from the controlled and intracellular release of the two payloads of DOX and siRNA from GQD/DOX/BCPV/siRNA nanocomplexes was capable of effectively inhibiting MiaPaCa-2 cells from aggressively growing to the corresponding cell colonies. GQD/DOX/BCPV/siRNA nanocomplexes therefore are considered a highly potent formulation to further have a great therapeutic efficiency in an in vivo model. As a result, relevant in vivo tests for the nanocomplexes are underway in our laboratory.

4. CONCLUSIONS

Taken together, GQD/DOX/BCPV/siRNA nanocomplexes have demonstrated their capability of simultaneous delivery of anticancer drug DOX and gene therapeutic agent siRNA into MiaPaCa-2 cells. Because of the photothermal effect, the two payloads can be selectively released at a desired site and a predetermined time via the laser light trigger. Using the nanocomplexes as the therapeutic formulation, the K-ras gene expression of MiaPaCa-2 cells was effectively suppressed, further leading to obvious inhibition in the cell bioactivities such as proliferation, cell migration, and invasion. More importantly, the anticancer activities of the nanocomplexes were significantly improved by irradiating them with proper laser light to release the DOX and siRNA. GQD/DOX/BCPV/siRNA nanocomplexes were supposed to have a promising potential for in vivo performance based on the cell colony formation results. With high biocompatibility, low biotoxicity, great delivery efficiency, and controllable release property, GQD/DOX/BCPV/siRNA nanocomplexes are considered to be as an ideal drug/gene delivery platform for various cancer therapies in future.

■ ASSOCIATED CONTENT

Supporting Information

The Supporting Information is available free of charge on the ACS Publications website at DOI: 10.1021/acsami.8b16168.

Photoluminescence spectra of the GQDs; chemical structure of BCPV; cytotoxicity of GQDs and BCPV; drug loading efficiency of GQDs; agarose gel electrophoresis analysis on the formation of GQD/DOX/BCPV/siRNA nanocomplexes; flow cytometry analysis on the transfection efficiency of the GQD/DOX/BCPV/siRNA nanocomplexes in MiaPaCa-2 cells; flow cytometry analysis on the apoptotic state of MiaPaCa-2 cells after treated with different formulations; temperature-increased profiles of the various GQD-based nanocomplexes under laser irradiation; photothermal therapeutic effect of GQD/BCPV on MiaPaCa-2 cells; and flow cytometry analysis on the light-triggering release of siRNA^{FAM} and DOX from intracellular GQD/DOX/BCPV/siRNA^{FAM} nanocomplexes (PDF)

■ AUTHOR INFORMATION

Corresponding Authors

*E-mail: xugaixia@szu.edu.cn (G.X.).
*E-mail: chihkuan@yuntech.edu.tw (C.-K.C.).
*E-mail: ktyong@ntu.edu.sg (K.-T.Y.).

ORCID

Chengbin Yang: 0000-0001-9672-7412
Kok Ken Chan: 0000-0002-0592-4427
Muhammad Danang Birowosuto: 0000-0002-9997-6841
Shuwen Zeng: 0000-0003-2188-7213
Takashi Ogi: 0000-0003-3982-857X
Chih-Kuang Chen: 0000-0002-7896-2424

DOI: 10.1021/acsami.8b16168
ACS Appl. Mater. Interfaces 2019, 11, 2768−2781

Ken-Tye Yong: 0000-0001-7936-2941

Author Contributions

K.-T.Y., C.-K.C., G.X., and C.Y. conceived and designed the project. M.D.B., S.Z., F.A.P., F.I., T.O., and K.O. synthesized the GQDs. C.Y., W.-J.L., and C.-K.C. designed and synthesized the BCPV. C.Y., K.K.C., M.Y., G.L., and X.W. performed the biological experiments and analyzed all data. C.Y. wrote the manuscript with the help of K.-T.Y. and C.-K.C. All authors discussed the results.

Notes

The authors declare no competing financial interest.

■ ACKNOWLEDGMENTS

This work was supported by the Singapore Ministry of Education (Grants Tier 2 MOE2010-T2-2-010 (M4020020.040 ARC2/11), the NTU-NHG Innovation Collaboration Grant (M4061202.040), the NTU-A*STAR Silicon Technologies, Centre of Excellence, under the program grant no. 11235100003, the NEWRI seed funding (grant no. NEWRI SF20140901), the research grants (nos. MOST 106-2221-E-224-058-; MOST 107-2221-E-224-059-MY2) supported by the Ministry of Science and Technology of Taiwan, and the grants from the National Natural Science Foundation of China (NSFC) (81400591). The authors thank for the help on the data analysis from Dr. Yining Lin at Shenzhen University. The authors also gratefully acknowledge the support from Instrumental Analysis Center of Shenzhen University.

■ REFERENCES

(1) Siegel, R. L.; Miller, K. D.; Jemal, A. Cancer statistics, 2018. *Ca-Cancer J. Clin.* **2018**, *68*, 7−30.

(2) Holohan, C.; Van Schaeybroeck, S.; Longley, D. B.; Johnston, P. G. Cancer drug resistance: an evolving paradigm. *Nat. Rev. Cancer* **2013**, *13*, 714−726.

(3) Yin, F.; Yang, C.; Wang, Q.; Zeng, S.; Hu, R.; Lin, G.; Tian, J.; Hu, S.; Lan, R. F.; Yoon, H. S.; Lu, F.; Wang, K.; Yong, K.-T. Light-driven therapy of pancreatic adenocarcinoma using gold nanorods-based nanocarriers for co-delivery of doxorubicin and siRNA. *Theranostics* **2015**, *5*, 818−833.

(4) Fan, W.; Yung, B.; Huang, P.; Chen, X. Nanotechnology for multimodal synergistic cancer therapy. *Chem. Rev.* **2017**, *117*, 13566−13638.

(5) Wang, S.; Lin, J.; Wang, Z.; Zhou, Z.; Bai, R.; Lu, N.; Liu, Y.; Fu, X.; Jacobson, O.; Fan, W.; Qu, J.; Chen, S.; Wang, T.; Huang, P.; Chen, X. Core-Satellite Polydopamine-Gadolinium-Metallofullerene Nanotheranostics for Multimodal Imaging Guided Combination Cancer Therapy. *Adv. Mater.* **2017**, *29*, 1701013.

(6) Tang, S.; Meng, Q.; Sun, H.; Su, J.; Yin, Q.; Zhang, Z.; Yu, H.; Chen, L.; Chen, Y.; Gu, W.; Li, Y. Tumor-microenvironment-adaptive nanoparticles codeliver paclitaxel and siRNA to inhibit growth and lung metastasis of breast cancer. *Adv. Funct. Mater.* **2016**, *26*, 6033−6046.

(7) Yang, C.; Hu, R.; Anderson, T.; Wang, Y.; Lin, G.; Law, W.-C.; Lin, W.-J.; Nguyen, Q. T.; Toh, H. T.; Yoon, H. S.; Chen, C.-K.; Yong, K.-T. nanoparticle-mediated K-ras down regulation for pancreatic cancer gene therapy. *J. Mater. Chem. B* **2015**, *3*, 2163−2172.

(8) Fleming, J. B.; Shen, G.-L.; Holloway, S. E.; Davis, M.; Brekken, R. A. Molecular Consequences of Silencing Mutant K-ras in Pancreatic Cancer Cells: Justification for K-ras-Directed Therapy. *Mol. Cancer Res.* **2005**, *3*, 413−423.

(9) Yang, C.; Chan, K. K.; Lin, W.-J.; Soehartono, A. M.; Lin, G.; Toh, H.; Yoon, H. S.; Chen, C.-K.; Yong, K.-T. Biodegradable nanocarriers for small interfering ribonucleic acid (siRNA) co-delivery strategy increase the chemosensitivity of pancreatic cancer cells to gemcitabine. *Nano Res.* **2017**, *10*, 3049−3067.

(10) Hu, R.; Yang, C.; Wang, Y.; Lin, G.; Qin, W.; Ouyan, Q.; Law, W.-C.; Nguyen, Q. T.; Yoon, H. S.; Wang, X.; Yong, K.-T.; Tang, B. Z. -induced emission (AIE) dye loaded polymer nanoparticles for gene silencing in pancreatic cancer and their in vitro and in vivo biocompatibility evaluation. *Nano Res.* **2014**, *8*, 1563−1576.

(11) Wang, Y.; Hu, R.; Lin, G.; Roy, I.; Yong, K.-T. Functionalized quantum dots for biosensing and bioimaging and concerns on toxicity. *ACS Appl. Mater. Interfaces* **2013**, *5*, 2786−2799.

(12) Wang, Y.; Wu, B.; Yang, C.; Liu, M.; Sum, T. C.; Yong, K.-T. Synthesis and Characterization of Mn:ZnSe/ZnS/ZnMnS Sandwiched QDs for Multimodal Imaging and Theranostic Applications. *Small* **2015**, *12*, 534−546.

(13) Wang, Y.; Yang, C.; Hu, R.; Toh, H. T.; Liu, X.; Lin, G.; Yin, F.; Yoon, H. S.; Yong, K.-T. Assembling Mn:ZnSe quantum dots-siRNA nanoplexes for gene silencing in tumor cells. *Biomater. Sci.* **2015**, *3*, 192−202.

(14) Zhang, B.; Yang, C.; Gao, Y.; Wang, Y.; Bu, C.; Hu, S.; Liu, L.; Demir, H. V.; Qu, J.; Yong, K.-T. Engineering quantum dots with different emission wavelengths and specific fluorescence lifetimes for spectrally and temporally multiplexed imaging of cells. *Nano-theranostics* **2017**, *1*, 131−140.

(15) Zhang, B.; Wang, Y.; Yang, C.; Hu, S.; Gao, Y.; Zhang, Y.; Wang, Y.; Demir, H. V.; Liu, L.; Yong, K.-T. The composition effect on the optical properties of aqueous synthesized Cu-In-S and Zn-Cu-In-S quantum dot nanocrystals. *Phys. Chem. Chem. Phys.* **2015**, *17*, 25133−25141.

(16) Iannazzo, D.; Ziccarelli, I.; Pistone, A. Graphene quantum dots: multifunctional nanoplatforms for anticancer therapy. *J. Mater. Chem. B* **2017**, *5*, 6471−6489.

(17) Wang, J.; Liu, J. PEI-folic acid modified carbon nanodots for cancer cell-targeted delivery and two-photon excitation imaging. *RSC Adv.* **2016**, *6*, 19662−19668.

(18) Jiang, K.; Sun, S.; Zhang, L.; Lu, Y.; Wu, A.; Cai, C.; Lin, H. Red, green, and blue luminescence by carbon dots: full-color emission tuning and multicolor cellular imaging. *Angew. Chem., Int. Ed.* **2015**, *54*, 5360−5363.

(19) Prasad, R.; Chauhan, D. S.; Yadav, A. S.; Devrukhkar, J.; Singh, B.; Gorain, M.; Temgire, M.; Bellare, J.; Kundu, G. C.; Srivastava, R. A biodegradable fluorescent nanohybrid for photo-driven tumor diagnosis and tumor growth inhibition. *Nanoscale* **2018**, *10*, 19082−19091.

(20) Wang, Y.; Wang, H.; Liu, D.; Song, S.; Wang, X.; Zhang, H. Graphene oxide covalently grafted upconversion nanoparticles for combined NIR mediated imaging and photothermal/photodynamic cancer therapy. *Biomaterials* **2013**, *34*, 7715−7724.

(21) Yadav, N.; Kumar, N.; Prasad, P.; Shirbhate, S.; Sehrawat, S.; Lochab, B. Stable dispersions of covalently tethered polymer improved graphene oxide nanoconjugates as an effective vector for siRNA delivery. *ACS Appl. Mater. Interfaces* **2018**, *10*, 14577−14593.

(22) Abdullah-Al-Nahain; Lee, J.-E.; In, I.; Lee, H.; Lee, K. D.; Jeong, J. H.; Park, S. Y. Target delivery and cell imaging using hyaluronic acid-functionalized graphene quantum dots. *Mol. Pharm.* **2013**, *10*, 3736−3744.

(23) Gao, T.; Wang, X.; Yang, L.-Y.; He, H.; Ba, X.-X.; Zhao, J.; Jiang, F.-L.; Liu, Y. Red, yellow, and blue luminescence by graphene quantum dots: syntheses, mechanism, and cellular Imaging. *ACS Appl. Mater. Interfaces* **2017**, *9*, 24846−24856.

(24) Ding, H.; Zhang, F.; Zhao, C.; Lv, Y.; Ma, G.; Wei, W.; Tian, Z. Beyond a carrier: graphene quantum dots as a probe for programmatically monitoring anti-cancer drug delivery, release, and response. *ACS Appl. Mater. Interfaces* **2017**, *9*, 27396−27401.

(25) Ge, J.; Lan, M.; Zhou, B.; Liu, W.; Guo, L.; Wang, H.; Jia, Q.; Niu, G.; Huang, X.; Zhou, H.; Meng, X.; Wang, P.; Lee, C.-S.; Zhang, W.; Han, X. A graphene quantum dot photodynamic therapy agent with high singlet oxygen generation. *Nat. Commun.* **2014**, *5*, 4596.

DOI: 10.1021/acsami.8b16168
ACS Appl. Mater. Interfaces 2019, 11, 2768−2781

(26) Chong, Y.; Ma, Y.; Shen, H.; Tu, X.; Zhou, X.; Xu, J.; Dai, J.; Fan, S.; Zhang, Z. The in vitro and in vivo toxicity of graphene quantum dots. *Biomaterials* **2014**, *35*, 5041−5048.
(27) Liu, H.; Qiu, J. C.; Zhang, R.; Li, J.; Sang, Y.; Tang, W.; Gil, P. R. Fluorescent graphene quantum dots as traceable, pH-sensitive drug delivery systems. *Int. J. Nanomed.* **2015**, *10*, 6709−6724.
(28) Wang, L.; Wang, Y.; Xu, T.; Liao, H.; Yao, C.; Liu, Y.; Li, Z.; Chen, Z.; Pan, D.; Sun, L.; Wu, M. Gram-scale synthesis of single-crystalline graphene quantum dots with superior optical properties. *Nat. Commun.* **2014**, *5*, 5357.
(29) Ogi, T.; Iwasaki, H.; Aishima, K.; Iskandar, F.; Wang, W.-N.; Takimiya, K.; Okuyama, K. Transient nature of graphene quantum dot formation via a hydrothermal reaction. *RSC Adv.* **2014**, *4*, 55709−55715.
(30) Permatasari, F. A.; Fukazawa, H.; Ogi, T.; Iskandar, F.; Okuyama, K. Design of pyrrolic-N-rich carbon dots with absorption in the first near-infrared window for photothermal therapy. *ACS Appl. Nano Mater.* **2018**, *1*, 2368−2375.
(31) Orecchioni, M.; Cabizza, R.; Bianco, A.; Delogu, L. G. Graphene as cancer theranostic tool: progress and future challenges. *Theranostics* **2015**, *5*, 710−723.
(32) Permatasari, F. A.; Aimon, A. H.; Iskandar, F.; Ogi, T.; Okuyama, K. Role of C−N configurations in the photoluminescence of graphene quantum dots synthesized by a hydrothermal route. *Sci. Rep.* **2016**, *6*, 21042.
(33) Chen, W.; Lv, G.; Hu, W.; Li, D.; Chen, S.; Dai, Z. Synthesis and applications of graphene quantum dots: a review. *Nanotechnol. Rev.* **2018**, *7*, 157−185.
(34) Du, X.; Shi, B.; Liang, J.; Bi, J.; Dai, S.; Qiao, S. Z. Developing Functionalized Dendrimer-Like Silica Nanoparticles with Hierarchical Pores as Advanced Delivery Nanocarriers. *Adv. Mater.* **2013**, *25*, 5981−5985.
(35) Jones, C. H.; Chen, C.-K.; Jiang, M.; Fang, L.; Cheng, C.; Pfeifer, B. A. Synthesis of cationic polylactides with tunable charge densities as nanocarriers for effective gene delivery. *Mol. Pharmaceutics* **2013**, *10*, 1138−1145.
(36) Chen, C.-K.; Jones, C. H.; Mistriotis, P.; Yu, Y.; Ma, X.; Ravikrishnan, A.; Jiang, M.; Andreadis, S. T.; Pfeifer, B. A.; Cheng, C. Poly(ethylene glycol)-block-cationic polylactide nanocomplexes of differing charge density for gene delivery. *Biomaterials* **2013**, *34*, 9688−9699.
(37) Pozzi, D.; Colapicchioni, V.; Caracciolo, G.; Piovesana, S.; Capriotti, A. L.; Palchetti, S.; De Grossi, S.; Riccioli, A.; Amenitsch, H.; Laganà, A. Effect of polyethyleneglycol (PEG) chain length on the bio-nano-interactions between PEGylated lipid nanoparticles and biological fluids: from nanostructure to uptake in cancer cells. *Nanoscale* **2014**, *6*, 2782−2792.
(38) Yang, C.; Panwar, N.; Wang, Y.; Zhang, B.; Liu, M.; Toh, H.; Yoon, H. S.; Tjin, S. C.; Chong, P. H. J.; Law, W.-C.; Chen, C.-K.; Yong, K.-T. charged polyester-based vectors (BCPVs) as an efficient non-viral transfection nanoagent for gene knockdown of the BCR−ABL hybrid oncogene in a human chronic myeloid leukemia cell line. *Nanoscale* **2016**, *8*, 9405−9416.
(39) Chen, C.-K.; Law, W.-C.; Aalinkeel, R.; Nair, B.; Kopwitthaya, A.; Mahajan, S. D.; Reynolds, J. L.; Zou, J.; Schwartz, S. A.; Prasad, P. N.; Cheng, C. Well-defined degradable cationic polylactide as nanocarrier for the delivery of siRNA to silence angiogenesis in prostate Cancer. *Adv. Healthcare Mater.* **2012**, *1*, 751−761.
(40) Lin, G.; Yang, C.; Hu, R.; Chen, C.-K.; Law, W.-C.; Anderson, T.; Zhang, B.; Nguyen, Q. T.; Toh, H. T.; Yoon, H. S.; Cheng, C.; Yong, K.-T. Interleukin-8 gene silencing on pancreatic cancer cells using biodegradable polymer nanoplexes. *Biomater. Sci.* **2014**, *2*, 1007−1015.
(41) Chang, Y.-T.; Liao, P.-Y.; Sheu, H.-S.; Tseng, Y.-J.; Cheng, F.-Y.; Yeh, C.-S. Near-Infrared Light-Responsive Intracellular Drug and siRNA Release Using Au Nanoensembles with Oligonucleotide-Capped Silica Shell. *Adv. Mater.* **2012**, *24*, 3309−3314.
(42) Luo, G.; Chen, W.; Jia, H.; Sun, Y.; Cheng, H.; Zhuo, R.; Zhang, X. An indicator-guided photo-controlled drug delivery system based on mesoporous silica/gold nanocomposites. *Nano Res.* **2015**, *8*, 1893−1905.
(43) Song, X.; Chen, Q.; Liu, Z. Recent advances in the development of organic photothermal nano-agents. *Nano Res.* **2014**, *8*, 340−354.
(44) Liu, T.; Chao, Y.; Gao, M.; Liang, C.; Chen, Q.; Song, G.; Cheng, L.; Liu, Z. Ultra-small MoS2 nanodots with rapid body clearance for photothermal cancer therapy. *Nano Res.* **2016**, *9*, 3003−3017.
(45) Wang, N.; Zhao, Z.; Lv, Y.; Fan, H.; Bai, H.; Meng, H.; Long, Y.; Fu, T.; Zhang, X.; Tan, W. Gold nanorod-photosensitizer conjugate with extracellular pH-driven tumor targeting ability for photothermal/photodynamic therapy. *Nano Res.* **2014**, *7*, 1291−1301.
(46) Wang, P.; Zhang, L.; Zheng, W.; Cong, L.; Guo, Z.; Xie, Y.; Wang, L.; Tang, R.; Feng, Q.; Hamada, Y.; Gonda, K.; Hu, Z.; Wu, X.; Jiang, X. Thermo-triggered release of CRISPR-Cas9 system by lipid-encapsulated gold nanoparticles for tumor therapy. *Angew. Chem., Int. Ed.* **2018**, *57*, 1491−1496.
(47) Yang, Y.; Velmurugan, B.; Liu, X.; Xing, B. NIR photo-responsive crosslinked upconverting nanocarriers toward selective intracellular drug release. *Small* **2013**, *9*, 2937−2944.
(48) Sun, X.; Wang, C.; Gao, M.; Hu, A.; Liu, Z. Remotely controlled red blood cell carriers for cancer targeting and near-infrared light-triggered drug release in combined photothermal-chemotherapy. *Adv. Funct. Mater.* **2015**, *25*, 2386−2394.
(49) Qiu, M.; Wang, D.; Liang, W.; Liu, L.; Zhang, Y.; Chen, X.; Sang, D. K.; Xing, C.; Li, Z.; Dong, B.; Xing, F.; Fan, D.; Bao, S.; Zhang, H.; Cao, Y. Novel concept of the smart NIR-light-controlled drug release of black phosphorus nanostructure for cancer therapy. *Proc. Natl. Acad. Sci. U.S.A.* **2018**, *115*, 501−506.
(50) Yao, C.; Wang, P.; Li, X.; Hu, X.; Hou, J.; Wang, L.; Zhang, F. Near-infrared-triggered azobenzene-liposome/upconversion nanoparticle hybrid vesicles for remotely controlled drug delivery to overcome cancer multidrug resistance. *Adv. Mater.* **2016**, *28*, 9341−9348.
(51) Su, J.; Sun, H.; Meng, Q.; Yin, Q.; Zhang, P.; Zhang, Z.; Yu, H.; Li, Y. Bioinspired Nanoparticles with NIR-Controlled Drug Release for Synergetic Chemophotothermal Therapy of Metastatic Breast Cancer. *Adv. Funct. Mater.* **2016**, *26*, 7495−7506.
(52) Panwar, N.; Yang, C.; Yin, F.; Yoon, H. S.; Chuan, T. S.; Yong, K.-T. RNAi-based therapeutic nanostrategy: IL-8 gene silencing in pancreatic cancer cells using gold nanorods delivery vehicles. *Nanotechnology* **2015**, *26*, 365101.
(53) Yang, C.; Mo, X.; Lv, J.; Liu, X.; Yuan, M.; Dong, M.; Li, L.; Luo, X.; Fan, X.; Jin, Z.; Liu, Z.; Liu, J. Lipopolysaccharide enhances Fc epsilon RI-mediated mast cell degranulation by increasing Ca2+ entry through store-operated Ca2+ channels: implications for lipopolysaccharide exacerbating allergic asthma. *Exp. Physiol.* **2012**, *97*, 1315−1327.
(54) Ma, Y.; Yu, S.; Zhao, W.; Lu, Z.; Chen, J. miR-27a regulates the growth, colony formation and migration of pancreatic cancer cells by targeting Sprouty2. *Cancer Lett.* **2010**, *298*, 150−158.
(55) Franken, N. A. P.; Rodermond, H. M.; Stap, J.; Haveman, J.; van Bree, C. Clonogenic assay of cells in vitro. *Nat. Protoc.* **2006**, *1*, 2315−2319.
(56) Lin, G.; Yang, C.; Hu, R.; Chen, C.-K.; Law, W.-C.; Anderson, T.; Zhang, B.; Nguyen, Q. T.; Toh, H. T.; Yoon, H. S.; Cheng, C.; Yong, K.-T. Interleukin-8 gene silencing on pancreatic cancer cells using biodegradable polymer nanoplexes. *Biomater. Sci.* **2014**, *2*, 1007−1015.
(57) Kim, H. J.; Kim, A.; Miyata, K.; Kataoka, K. Recent progress in development of siRNA delivery vehicles for cancer therapy. *Adv. Drug Delivery Rev.* **2016**, *104*, 61−77.
(58) Whitehead, K. A.; Langer, R.; Anderson, D. G. Knocking down barriers: advances in siRNA delivery. *Nat. Rev. Drug Discovery* **2009**, *8*, 129−138.
(59) Amjad, M. W.; Kesharwani, P.; Mohd Amin, M. C. I.; Iyer, A. K. Recent advances in the design, development, and targeting mechanisms of polymeric micelles for delivery of siRNA in cancer therapy. *Prog. Polym. Sci.* **2017**, *64*, 154−181.

DOI: 10.1021/acsami.8b16168
ACS Appl. Mater. Interfaces 2019, 11, 2768−2781

(60) Xu, W.; Wang, Z.; Zhang, W.; Qian, K.; Li, H.; Kong, D.; Li, Y.; Tang, Y. Mutated K-ras activates CDK8 to stimulate the epithelial-to-mesenchymal transition in pancreatic cancer in part via the Wnt/β-catenin signaling pathway. *Cancer Lett.* **2015**, *356*, 613−627.
(61) Judson, I.; Verweij, J.; Gelderblom, H.; Hartmann, J. T.; Schöffski, P.; Blay, J.-Y.; Kerst, J. M.; Sufliarsky, J.; Whelan, J.; Hohenberger, P. alone versus intensified doxorubicin plus ifosfamide for first-line treatment of advanced or metastatic soft-tissue sarcoma: a randomised controlled phase 3 trial. *Lancet Oncol.* **2014**, *15*, 415−423.
(62) Eke, I.; Hehlgans, S.; Sandfort, V.; Cordes, N. 3D matrix-based cell cultures: Automated analysis of tumor cell survival and proliferation. *Int. J. Oncol.* **2015**, *48*, 313−321.
(63) Katt, M. E.; Placone, A. L.; Wong, A. D.; Xu, Z. S.; Searson, P. C. In vitro tumor models: advantages, disadvantages, variables, and selecting the right platform. *Front. Biotechnol. Bioeng.* **2016**, *4*, 12.

DOI: 10.1021/acsami.8b16168
ACS Appl. Mater. Interfaces 2019, 11, 2768−2781